Received June 22, 2018, accepted July 14, 2018, date of publication July 19, 2018, date of current version August 15, 2018.

Digital Object Identifier 10.1109/ACCESS.2018.2857458

A High-Bandwidth and Strong Robust Current Control Strategy for PMLSM Drives

MING-YI WANG, RUI YANG, (Student Member, IEEE), QIANG TAN, JI-WEI CAO, CHENG-MING ZHANG, AND LI-YI LI, (Member, IEEE)

Department of Electrical Engineering, Harbin Institute of Technology, Harbin 150001, China

Corresponding author: Ming-Yi Wang (hit_mywang@163.com)

This work was supported in part by the National Natural Science Foundation of China under Grant 51707046, in part by the Self-Planned Task of State Key Laboratory of Robotics and System under Grant SKLRS201711A, in part by the State Key Program of National Natural Science of China under Grant 51537002, and in part by the State Major Program of National Natural Science of China under Grant 51690182.

ABSTRACT As an ideal current control method, the superiority of the predictive current control (PCC) is seriously weakened by the one-step control delay and parameter mismatch issues. To acquire the high dynamic and static characteristics, this paper studies an improved PCC scheme for the permanent magnet linear synchronous motor (PMLSM) drives. First, the discrete-time model of PMLSM considering the parameter variation is established. Second, the formation mechanisms of these two issues are analyzed in detail, respectively. Meanwhile, through replanning the timing sequence logic, the one-step control delay issue is solved. Furthermore, based on the super-twisting algorithm, the super-twisting sliding-mode observer (STSMO) is constructed to compensate for the parameter disturbance. To further improve the dynamic property and lower the chattering, a third-order STSMO is presented in comparison with the second-order STSMO. In the meantime, the estimated currents can be utilized in the solution of one-step delay issue. At last, on the PMLSM testing platform based on the aerostatic guide, the corresponding experimental results are shown to verify the effectiveness and correctness of the proposed method.

INDEX TERMS Permanent magnet linear synchronous motor (PMLSM), predictive control, one-step delay, parameter mismatch, sliding-mode.

NOMENCLATURE

v_q, v_d	q- and d-axis voltages.
i_q, i_d	q- and d-axis currents.
R	Phase winding resistance.
L_q, L_d	q- and d-axis inductances.
λ_f	Permanent magnet flux linkage.
λ_q, λ_d	q- and d-axis magnet flux linkages.
v	Linear velocity of the mover.
ζ_q, ζ_d	q- and d-axis disturbance voltages.
T_s	Switching period.
τ	Pole pitch.
p	Pole pairs.

I. INTRODUCTION

Recently, the rapid development of manufacturing industry promotes the widespread application of permanent magnet linear synchronous motor (PMLSM) because of its advantages of high dynamic response, high efficiency and force density [1]. As the power source, the control performance of PMLSM is extremely important for developing the high-end equipments. Among different control schemes of PMLSM drives, most of thrust control methods are based on regulating the motor phase current, which means the current loop is essential to the PMLSM control system [2].

An ideal current controller for PMLSM not only has characteristics of high bandwidth and high tracking precision, but also has the ability to avoid d-q axis coupling, back electromotive force (EMF) and parameter disturbances. In motor drives, the current control includes the following strategies: hysteresis control, proportional-integral (PI) control and predictive control [3]. In the early studies, the hysteresis control is widely used in motor drives because of its advantages such as high dynamic response, easy realization, and simple principle [4]. However, the inconstant switching frequency, large electromagnetic noise and current ripple are inevitable [5]. Generally, the hysteresis control is limited in the field of the high-performance motor drives. With the development

of digital control system, PI control gradually becomes the most pervasive method in the motor servo system. The main advantages of PI control are the constant switching frequency, strong robustness and stability [6], but the performance degradation with the PI controller is difficult to be avoided if the control system faces different operation conditions, such as load or parameter variations. Otherwise, the PI controller in current loop generally ignores the d-q axis coupling [7] and back electromotive force (EMF) disturbance problems. Compared with hysteresis control and PI control, the predictive current control (PCC) method has more outstanding static and dynamic performances [8], [9]. Theoretically, by using the PCC method, the actual current can track its command during one switching period precisely. What is more, as the model-based algorithm, the PCC overcomes the coupling and EMF disturbance problems. Therefore, the PCC method is very suitable for the high-performance current control.

Nevertheless, two main issues have to be considered in the PCC application [10]. One is the one-step delay problem. In the digital control system, there is one switching period delay for the command voltage in the process from calculating to loading, which will cause the overshoot or even oscillation. The other is the parameter mismatch problem. PCC is based on the motor model, so it is sensitive to the motor parameter. If the parameters set in controller are different from the actual ones or the motor parameters change with the operating situation, the control performance will be deteriorated. For this reason, a lot of researches focus on these two issues. For the one-step delay issue, [10] has analyzed its forming reason, and proposed to overcome this delay by calculating the voltage command of the next switching period. However, in the implementation process, most studies usually neglect the importance of the sampling currents of next period, which are usually achieved by using the rough estimation method. Additionally, because of powerful real-time and parallel computing abilities, some hardware technologies are used to overcome the delay issue [11]. But a lot of engineering design cost complicates the implementation of PCC.

For the parameter mismatch issue, it is necessary to study the robust current control method. In the survey of disturbance or uncertainty in motor drives, [12] summarizes the parametric uncertainties, and the nonlinear disturbance observer-based control (NDOBC) is applied to estimate and compensate the uncertainties. As the main PCC method, the model predictive control (MPC) with different robust algorithms is widely studied. A Lyapunov-based MPC [13] is proposed to enhance the robust stability for PMSM drives by introducing the contraction constraint. MPC based on Takagi-Sugeno fuzzy model [14], [15] is proposed, and this study can effectively strengthen the robustness of non-linear delayed systems, and this method is successfully applied in the electric vehicle (EV) system. In [16], the current tracking precision is improved by proposing a current error correction technique, and the dynamic performance is enhanced by introducing a current-regulated delta modulator. Similarly, the prediction errors with a weighting factor are added to the prediction stage, the robustness of PCC against parameter uncertainties is promoted by using the prediction error correction technology [17].The online parameter identification method has been researched to estimate the motor parameters. In [18], by introducing the self-adaptive learning bat-inspired algorithm, the parameters can be accurately identified in the nonlinear chaotic system. In [19], the disturbance observer based on the time delay control is proposed to solve the parameter mismatch issue,. Recently, the robust controller based on the uncertainty and disturbance estimator (UDE) is proposed to replace the time delay control [20].In [21], a discrete-time integral term is added to PCC, and this method can provide the robustness against the parameter variations with a simple structure. Among various disturbance observers, due to the strong robustness and fast convergence, the sliding-mode observer (SMO) is well suited to compensate the parameter variation or overcome the system uncertainty [22]–[25]. In [22], SMO based on the exponential reaching law is presented to estimate the parameter variations in PCC. To suppress the chattering, this paper optimizes the exponential reaching law. In addition, in [23], [24], and [25], various SMOs are also presented to suppress the parameter uncertainties of different systems. In recent years, the SMO based on the super-twisting (ST) algorithm has many advantages such as faster convergence ability and lower chattering effect. Therefore, some STSMOs, especially the high-order STSMO, generally become the research focus [26]–[28]. In [26], a second-order STSMO is designed to estimate the parameter variations for induction machine drives. Since the high-order SMO has lower chattering and more excellent dynamic performance, [27] and [28] both choose the high-order SMO to solve the system uncertainties.

A. MAIN CONTRIBUTION

To realize the high bandwidth and high tracking accuracy of the current closed-loop, the predictive control strategy is a very appropriate choice in several common methods. However, only if two main problems (one-step delay and parameter mismatch) are effectively solved, PCC can have a more practical sense. Based on the presented STSMO, the sampling currents and parameter disturbance voltages at the beginning of next period are exactly estimated. The estimated currents are used in the calculation of voltage commands, thus one-step delay issue is overcome. In addition, the parameter disturbance voltages are injected into the current closed-loop through the feed forward method, the parameter mismatch issue is also addressed. What is more, the designed third-order STSMO has the better observation performance. Finally, we present a current controller with characteristics of high bandwidth and strong parameter robustness, which can be generalized for the high-performance motor drives.

B. STRUCTURE OF THIS PAPER

The structure of this paper is given as follows. Section II establishes the discrete-time model of PMLSM considering the parameter mismatch between the driven motor

and its controller. Section III analyzes one-step delay and parameter mismatch issues, and presents an improved PCC. In Section IV, the second-order STSMO is given to suppress the parameter disturbance, and through designing a third-order STSMO, the observation performance is obviously improved. In Section V, the explored approach is implemented in a precise PMLSM testing platform. At last, Section VI gives the conclusion.

II. PMLSM MODEL

Before establishing the mathematical model of PMLSM, it is necessary to give the following assumptions: the relative permeability of primary and secondary iron core is infinite, and the eddy current and hysteresis losses are ignored; in the air gap, the excitation and armature reaction magnetic field are the sinusoidal distribution; the flux distortions are neglected. The voltage equation can be expressed as

$$\begin{cases} v_q = R_o i_q + \dfrac{d\lambda_{qo}}{dt} + \dfrac{\pi v \lambda_{do}}{\tau} + \zeta_q \\ v_d = R_o i_d + \dfrac{d\lambda_{do}}{dt} - \dfrac{\pi v \lambda_{qo}}{\tau} + \zeta_d \end{cases} \tag{1}$$

where the subscript "o" denotes the nominal value, and λ_{qo}, λ_{do} can be defined as

$$\begin{cases} \lambda_{qo} = L_{qo} i_q \\ \lambda_{do} = L_{do} i_d + \lambda_{fo} \end{cases} \tag{2}$$

Since the motor parameters are influenced by the operating condition and other uncertainties, the parameter values may be different between the actual motor and its controller. Therefore, the parameter variation is deduced as

$$\begin{cases} \zeta_q = \Delta R i_q + \dfrac{\Delta L_q di_q}{dt} + \dfrac{\pi v \Delta L_d i_d}{\tau} + \dfrac{\pi v \Delta \lambda_f}{\tau} \\ \zeta_d = \Delta R i_d + \dfrac{\Delta L_d di_d}{dt} - \dfrac{\pi v \Delta L_q i_q}{\tau} \end{cases} \tag{3}$$

where ΔR, ΔL_q (ΔL_d) and $\Delta\lambda_f$ represent respective disturbances.

According to the voltage equation of (1), its discrete-time equation can be expressed in the form of the first-order Taylor series expansion if the sampling period is short enough, which means that

$$\begin{cases} v_q(k) = R_o i_q(k) + \dfrac{L_{qo}}{T_s}\left[i_q(k+1) - i_q(k)\right] \\ \qquad + \dfrac{\pi v L_{do}}{\tau} i_d(k) + \dfrac{\pi v \lambda_{fo}}{\tau} + \zeta_q(k) \\ v_d(k) = R_o i_d(k) + \dfrac{L_{do}}{T_s}\left[i_d(k+1) - i_d(k)\right] \\ \qquad - \dfrac{\pi v L_{qo}}{\tau} i_q(k) + \zeta_d(k). \end{cases} \tag{4}$$

Therefore, the dynamic equation of (4) can be represented in matrix form

$$\boldsymbol{V}(k) = \boldsymbol{G} \cdot \boldsymbol{I}(k) + \boldsymbol{H} \cdot \boldsymbol{I}(k+1) + \boldsymbol{\lambda} + \boldsymbol{D}(k) \tag{5}$$

where

$$\boldsymbol{V}(k) = \begin{bmatrix} v_q(k) & v_d(k) \end{bmatrix}^T, \quad \boldsymbol{I}(k) = \begin{bmatrix} i_q(k) & i_d(k) \end{bmatrix}^T,$$
$$\boldsymbol{\lambda} = \begin{bmatrix} \pi v \lambda_{fo}/\tau & 0 \end{bmatrix}^T, \quad \boldsymbol{D}(k) = \begin{bmatrix} \zeta_q(k) & \zeta_d(k) \end{bmatrix}^T,$$
$$\boldsymbol{G} = \begin{bmatrix} R_o - L_{qo}/T_s & \pi v L_{do}/\tau \\ -\pi v L_{qo}/\tau & R_o - L_{do}/T_s \end{bmatrix},$$
$$\boldsymbol{H} = \begin{bmatrix} L_{qo}/T_s & 0 \\ 0 & L_{do}/T_s \end{bmatrix}.$$

In order to facilitate the following analysis, the current vector at the beginning of the $(k+1)$th period in (5) is moved to the left of equation, which is shown as

$$\boldsymbol{I}(k+1) = \boldsymbol{G}_0 \cdot \boldsymbol{I}(k) + \boldsymbol{H}_0 \cdot [\boldsymbol{V}(k) - \boldsymbol{\lambda} - \boldsymbol{D}(k)] \tag{6}$$

where

$$\boldsymbol{G}_0 = \begin{bmatrix} 1 - R_o T_s/L_{qo} & -\pi v T_s/\tau \\ \pi v T_s/\tau & 1 - R_o T_s/L_{qo} \end{bmatrix},$$
$$\boldsymbol{H}_0 = \begin{bmatrix} T_s/L_{qo} & 0 \\ 0 & T_s/L_{qo} \end{bmatrix}.$$

III. PCC SCHEME AND ITS ISSUES

A. PCC WITH ONE-STEP DELAY ISSUE

Without considering the delay of the digital control, the voltage command $\boldsymbol{V}^*(k)$ is deduced in according to (5).

$$\boldsymbol{V}^*(k) = \boldsymbol{G} \cdot \boldsymbol{I}(k) + \boldsymbol{H} \cdot \boldsymbol{I}^*(k+1) + \boldsymbol{\lambda} + \boldsymbol{D}(k) \tag{7}$$

where the subscript "*" represents the command.

iF ignoring the disturbance vector $\boldsymbol{D}(k)$, theoretically, the actual current can track the command one after one sampling period. However, due to one-step delay in the digital control, $\boldsymbol{V}^*(k)$ is added to the inverter after one control period. Consequently, the actual current has a poor stability. The timing sequence and performance of PCC with the one-step delay issue are shown in Fig. 1.

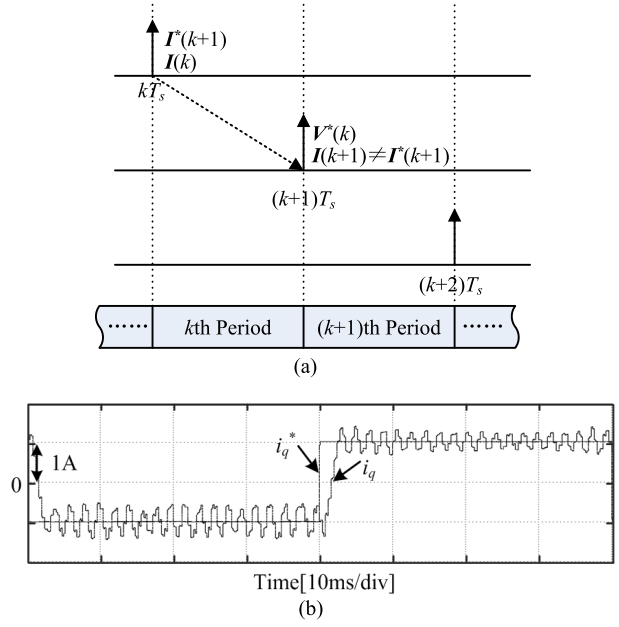

FIGURE 1. PCC without the one-step delay compensation. (a) Timing sequence diagram. (b) Current tracking Performance.

To overcome this problem, we can calculate the voltage command during the next period.

$$\boldsymbol{V}^*(k+1) = \boldsymbol{G}\cdot\boldsymbol{I}(k+1) + \boldsymbol{H}\cdot\boldsymbol{I}^*(k+2) + \boldsymbol{\lambda} + \boldsymbol{D}(k+1). \quad (8)$$

Since the actual current $\boldsymbol{I}(k+1)$ and parameter disturbance $\boldsymbol{D}(k+1)$ of next period are unknown, and we have to estimate them through some observation technology. Thus (8) is rewritten as

$$\boldsymbol{V}^*(k+1) = \boldsymbol{G}\cdot\hat{\boldsymbol{I}}(k+1) + \boldsymbol{H}\cdot\boldsymbol{I}^*(k+2) + \boldsymbol{\lambda} + \hat{\boldsymbol{D}}(k+1). \quad (9)$$

After the above analysis, the current command can be tracked after two sampling periods. The timing sequence and performance of PCC with the one-step delay compensation are shown in Fig. 2.

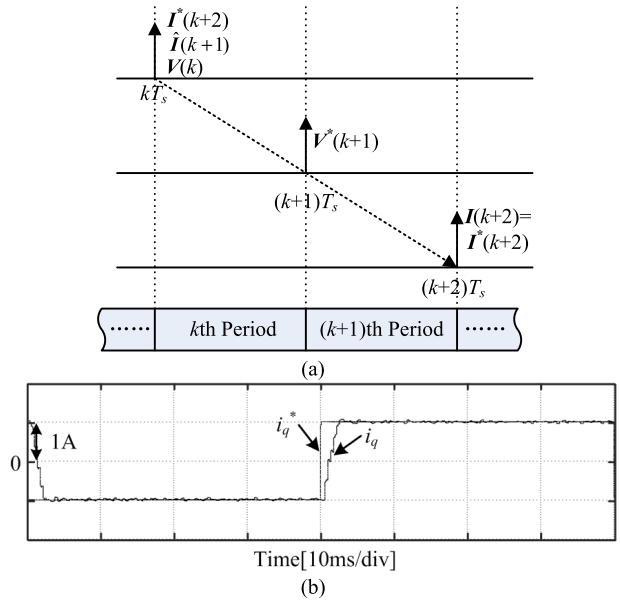

FIGURE 2. PCC with the one-step delay compensation. (a) Timing sequence diagram. (b) Current tracking Performance.

B. PARAMETER MISMATCH ISSUE

It is assumed that the actual voltage is equal to the command.

$$\boldsymbol{V}(k+1) = \boldsymbol{V}^*(k+1) \quad (10)$$

According to (5), $\boldsymbol{V}(k+1)$ satisfies the following relationship.

$$\boldsymbol{V}(k+1) = \boldsymbol{G}\cdot\boldsymbol{I}(k+1) + \boldsymbol{H}\cdot\boldsymbol{I}(k+2) + \boldsymbol{\lambda} + \boldsymbol{D}(k+1) \quad (11)$$

To analyze the influence of parameter disturbance, in the process of the controller design, it is assumed that $\hat{\boldsymbol{D}}(k+1)$ in (9) is ignored, and the estimated $\hat{\boldsymbol{I}}(k+1)$ is equal to its actual value $\boldsymbol{I}(k+1)$. Therefore, according to (9), (10) and (11), the tracking error is calculated as

$$\boldsymbol{I}^*(k+2) - \boldsymbol{I}(k+2) = \boldsymbol{H}^{-1}\cdot\boldsymbol{D}(k+1). \quad (12)$$

We can further express (12) in the following form.

$$\begin{cases} i_q^*(k+2) - i_q(k+2) = \dfrac{T_s}{L_{so}}\zeta_q(k+1) \\ i_d^*(k+2) - i_d(k+2) = \dfrac{T_s}{L_{so}}\zeta_d(k+1). \end{cases} \quad (13)$$

If the resistance changes (the disturbance value is ΔR), and the other parameters stay the same. According to (3) and (13), the tracking error is simplified as

$$\begin{cases} i_q^*(k+2) - i_q(k+2) = \dfrac{\Delta R T_s}{L_{so}} i_q(k+1) \\ i_d^*(k+2) - i_d(k+2) = \dfrac{\Delta R T_s}{L_{so}} i_d(k+1). \end{cases} \quad (14)$$

It is obvious there is a constant error after the current gets to a stable state, and it is proportional to the disturbance value ΔR. Hence the resistance variation reduces the current control precision.

If the inductance changes (the disturbance is ΔL), and the others remain unchanged, the error is expressed as

$$\begin{cases} i_q^*(k+2) - i_q(k+2) = \dfrac{\Delta L_q}{2L_{so}}\left(i_q(k+2) - i_q(k)\right) + \dfrac{\pi v \Delta L_d T_s}{\tau L_{so}} i_d(k+2) \\ i_d^*(k+2) - i_d(k+2) = \dfrac{\Delta L_d}{2L_{so}}\left(i_d(k+2) - i_d(k)\right) - \dfrac{\pi v \Delta L_q T_s}{\tau L_{so}} i_q(k+2). \end{cases} \quad (15)$$

On the right side of (15), it can be seen that the first term is related to the dynamic variation of the actual current, which means the inductance variation can affect the dynamic property of the current controller. In addition, the value of the second term is proportional to the velocity, d-axis or q-axis current. Because the controller adopts the field oriented control method with $i_d = 0$, the second term mainly brings d-axis current tracking error.

Similarly, only the flux linkage changes (the disturbance is $\Delta\lambda_f$), the error is given as

$$\begin{cases} i_q^*(k+2) - i_q(k+2) = \dfrac{\pi v T_s}{L_{so}\tau}\Delta\lambda f(k+1) \\ i_d^*(k+2) - i_d(k+2) = 0. \end{cases} \quad (16)$$

It is obvious that the d-axis current is not influenced under the flux linkage variation, but the tracking error of the q-axis current changes with the actual velocity. Basically, the error is proportional to the velocity.

IV. SUPER-TWISTING SLIDING-MODE OBSERVER DESIGN

According to the analysis in Section III, obviously, the accurate estimations of $\boldsymbol{I}(k+1)$ and $\boldsymbol{D}(k+1)$ take a critical part in the process of obtaining the high-performance PCC. Therefore, this section estimates $\boldsymbol{I}(k+1)$ and $\boldsymbol{D}(k+1)$ through designing the STSMO, and compared with the second-order STSMO, the observation performance of the third-order STSMO is significantly improved. As is well-known,

the electromagnetic thrust is proportional to the q-axis current if the air gap flux density is not saturated. Therefore, based on the field oriented control method with $i_d = 0$, this paper takes the q-axis current i_q as an example. Fig. 3 shows the block diagram of the proposed PCC with STSMO for PMLSM drives.

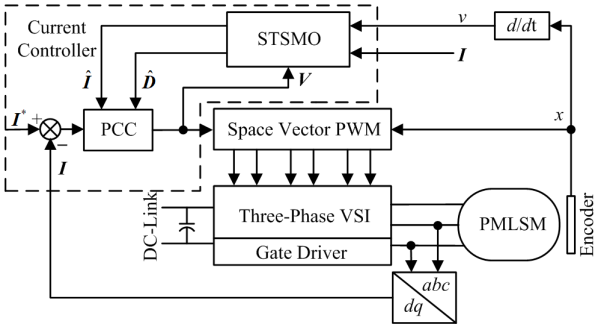

FIGURE 3. Block diagram of the proposed PCC with STSMO for PMLSM drives.

A. SECOND-ORDER STSMO

According to (6), when the parameter variation is taken into account, the state equation is established as

$$\begin{cases} \dfrac{di_q}{dt} = -\dfrac{R_o}{L_{qo}} i_q + \dfrac{v_q}{L_{qo}} - \dfrac{\pi v}{\tau L_{qo}} \left(L_{do} i_d + \lambda_{fo}\right) - \dfrac{\zeta_q}{L_{qo}} \\ \dfrac{d\zeta_q}{dt} = \rho\,(t) \end{cases} \tag{17}$$

where $\rho(t)$ is the derivative of ζ_q. Since the disturbance is continuous, there is a positive constant Δ which satisfies

$$|\rho\,(t)| \le \Delta. \tag{18}$$

Since the second-order STSMO was proposed by Levant [29], this algorithm has been widely used in the uncertain systems. Define the state error and the second-order STSMO dynamic equation as

$$e_1 = \hat{i}_q - i_q \tag{19}$$

$$\begin{cases} \dfrac{d\hat{i}_q}{dt} = -\dfrac{R_o}{L_{qo}} i_q + \dfrac{v_q}{L_{qo}} - \dfrac{\pi v}{\tau L_{qo}} \left(L_{do} i_d + \lambda_{fo}\right) \\ \qquad\qquad - \dfrac{\zeta_q}{L_{qo}} - k_1 \left|e_1\right|^{1/2} \mathrm{sgn}\,(e_1) \\ \dfrac{d\hat{\zeta}_q}{dt} = L_{qo} k_2 \mathrm{sgn}\,(e_1) \end{cases} \tag{20}$$

where e_1 is the error variable, $\hat{i}_q$ and $\hat{\zeta}_q$ are estimated values. Meanwhile, we define the second estimated error in the following form

$$e_2 = -\frac{\hat{\zeta}_q}{L_{qo}} + \frac{\zeta_q}{L_{qo}}. \tag{21}$$

At the initial moment, we can set the initial solutions as $\hat{i}_q = i_q$ and $\hat{\zeta}_q = 0$. The error dynamics can be expressed as

$$\begin{cases} \dfrac{de_1}{dt} = -k_1 \left|e_1\right|^{1/2} \mathrm{sgn}\,(e_1) + e_2 \\ \dfrac{de_2}{dt} = -k_2 \mathrm{sgn}\,(e_1) + \dfrac{\rho\,(t)}{L_{qo}}. \end{cases} \tag{22}$$

Due to $|\rho\,(t)| \le \Delta$, we can define a positive constant Δ_1 that satisfies $|\rho\,(t)| / L_{qo} \le \Delta / L_{qo} = \Delta_1$. We can see (22) is the same as the super twisting observer in [30] and [31], and based on the stability analysis proved in [30] and [31], we can use the conclusion that e_1 and e_2 will converge to zero in finite time if k_1 and k_2 are set as the following form

$$\begin{cases} k_1 > \sqrt{\dfrac{2}{k_2 - \Delta_1}} \dfrac{(k_2 + \Delta_1)\,(1+p)}{1-p} \\ k_2 > \Delta_1 \end{cases} \tag{23}$$

where p is a constant, and satisfies $0 < p < 1$.

To solve the two problems in PCC, $\boldsymbol{I}(k+1)$ and $\boldsymbol{D}(k+1)$ should be estimated, which means that the second-order STSMO has to be discretized. The discrete-time equation is expressed in the form of the first-order Taylor series expansion.

$$\begin{cases} \hat{i}_q\,(k+1) = T_s \Big[-\dfrac{R_o}{L_{qo}} i_q\,(k) + \dfrac{v_q\,(k)}{L_{qo}} \\ \qquad\qquad - \dfrac{\pi v\,(k)}{\tau L_{qo}} \left(L_{do} i_d\,(k) + \lambda_{fo}\right) \Big] \\ \qquad\qquad - \dfrac{T_s \hat{\zeta}_q\,(k)}{L_{qo}} - T_s k_1 |e_1(k)|^{1/2} \mathrm{sgn}\,(e_1\,(k)) + \hat{i}_q(k) \\ \hat{\zeta}_q\,(k+1) = T_s L_{qo} k_2 \mathrm{sgn}\,(e_1\,(k)) + \hat{\zeta}_q\,(k) \end{cases} \tag{24}$$

where $\hat{i}_q\,(k+1)$ and $\hat{\zeta}_q\,(k+1)$ are the corresponding estimations at the $(k+1)$th sampling instant, $v_q(k)$, $i_d(k)$, $v(k)$, and $e_1(k)$ are the corresponding estimations at the kth sampling instant, respectively. Fig. 4 shows the block diagram of the second-order STSMO.

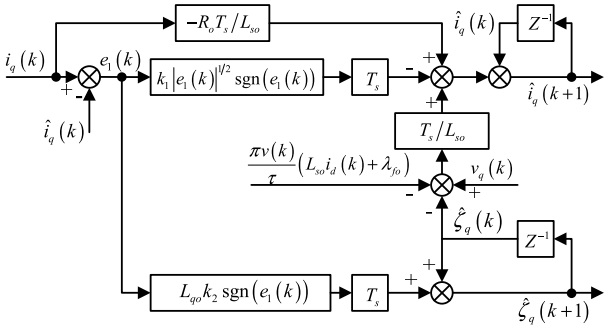

FIGURE 4. Block diagram of the second-order STSMO.

B. THIRD-ORDER STSMO

Although the one-step delay and parameter mismatch issues can be solved by combining the second-order STSMO,

the chattering problem brought by low-order SM has to be considered, and this problem can introduce a lot of electromagnetic noise and reduce the tracking precision. Therefore, this part constructs a third-order STSMO, which not only could observe $\boldsymbol{I}(k+1)$ and $\boldsymbol{D}(k+1)$ accurately and quickly, but also efficiently suppress the chattering problem. In addition, it is different from the second-order STSMO that the third-order STSMO also considers the derivative of parameter disturbance, which makes a more appropriate observation.

According to the state equation given in (17), the dynamic equation of the third-order STSMO is defined as

$$\begin{cases} \dfrac{d\hat{i}_q}{dt} = -\dfrac{R_o}{L_{qo}} i_q + \dfrac{v_q}{L_{qo}} - \dfrac{\pi v}{\tau L_{qo}} \left(L_{do} i_d + \lambda_{fo}\right) - \dfrac{\hat{\zeta}_q}{L_{qo}} \\ \qquad - k_1 \left|e_1\right|^{2/3} \operatorname{sgn}\left(e_1\right) \\ \dfrac{d\hat{\zeta}_q}{dt} = L_{qo} k_2 \left|e_1\right|^{1/3} \operatorname{sgn}\left(e_1\right) + \hat{\rho}\left(t\right) \\ \dfrac{d\hat{\rho}\left(t\right)}{dt} = L_{qo} k_3 \operatorname{sgn}\left(e_1\right) \end{cases} \tag{25}$$

If $\rho(t)$ is regarded as the third estimated value, the third estimated error is written as

$$e_3 = -\frac{\hat{\rho}\left(t\right)}{L_{qo}} + \frac{\rho\left(t\right)}{L_{qo}}. \tag{26}$$

At the initial moment, we can assume that the initial solutions are $\hat{i}_q = i_q$, $\hat{\zeta}_q = 0$, and $\rho(t_0) = 0$. The error dynamic can be deduced as

$$\begin{cases} \dfrac{de_1}{dt} = -k_1 \left|e_1\right|^{2/3} \operatorname{sgn}\left(e_1\right) + e_2 \\ \dfrac{de_2}{dt} = -k_2 \left|e_1\right|^{1/3} \operatorname{sgn}\left(e_1\right) + e_3 \\ \dfrac{de_3}{dt} = -k_3 \operatorname{sgn}\left(e_1\right) + \dfrac{\dot{\rho}\left(t\right)}{L_{qo}}. \end{cases} \tag{27}$$

According to [32]–[34], if $\rho(t)$ is a Lipschitz and $\left|\dot{\rho}\left(t\right)\right| / L_{qo} \leq \Delta_2$, (27) is stable, and the corresponding stability analysis has been discussed. Therefore, if choosing some appropriate positive k_1, k_2 and k_3 on the basis of [34], e_1, e_2 and e_3 will quickly converge to zero in finite time.

Then, the third-order STSMO dynamic equation is discretized as

$$\begin{cases} \hat{i}_q\left(k+1\right) = T_s \left[-\dfrac{R_o}{L_{qo}} i_q\left(k\right) + \dfrac{v_q\left(k\right)}{L_{qo}} \right. \\ \qquad \left. - \dfrac{\pi v\left(k\right)}{\tau L_{qo}} \left(L_{do} i_d\left(k\right) + \lambda_{fo}\right) \right] \\ \qquad - \dfrac{T_s \hat{\zeta}_q\left(k\right)}{L_{qo}} - T_s k_1 \left|e_1\left(k\right)\right|^{2/3} \operatorname{sgn}\left(e_1\left(k\right)\right) + \hat{i}_q\left(k\right) \\ \hat{\zeta}_q\left(k+1\right) = T_s L_{qo} k_2 \left|e_1\left(k\right)\right|^{1/3} \operatorname{sgn}\left(e_1\left(k\right)\right) \\ \qquad + T_s \hat{\rho}\left(k\right) + \hat{\zeta}_q\left(k\right) \\ \hat{\rho}\left(k+1\right) = T_s L_{qo} k_3 \operatorname{sgn}\left(e_1\left(k\right)\right) + \hat{\rho}\left(k\right). \end{cases} \tag{28}$$

To understand the third-order STSMO clearly, its block diagram is depicted in Fig. 5.

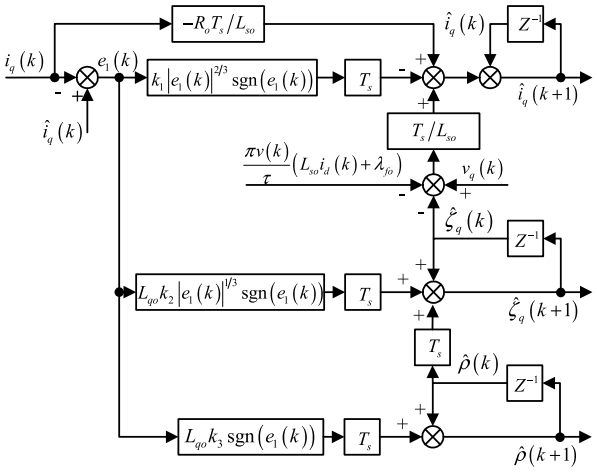

FIGURE 5. Block diagram of the third-order STSMO.

V. EXPERIMENTAL VERIFICATION

To verify the validity of the proposed method, a precise testing platform with the aerostatic guide is built, as shown as Fig. 6. The testing motor is the iron core PMLSM. The moving primary is installed on the mover of the linear guide. The position sensor adopts Renishaw linear incremental encoder with a resolution of 0.1 [μm].

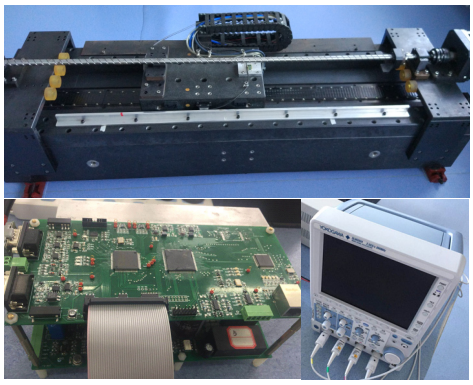

FIGURE 6. Experimental platform of the PMLSM system.

The testing PMLSM is driven by the voltage source inverter, and a DSP-based controller is designed to implement the proposed algorithm. The selected TMS320F28335 is a 32-bit floating-point DSP, and has 150 [MHz] of high-speed operation capacity. In addition, a XC3S50 FPGA is utilized to realize some functions including fault diagnosing and interface configuring. The experimental data are displayed on the oscilloscope by a 12-bit DA converter. The block diagram of the experimental platform is shown in Fig. 7. The main parameters of PMLSM are given in Table 1.

Based on the SVPWM technology, the voltage command can be loaded to the PMLSM, and the switching frequency is set to 5 [kHz]. In the experimental process, under the condition of the parameter match or mismatch, the results of the q-axis current tracking performance with the PCC method

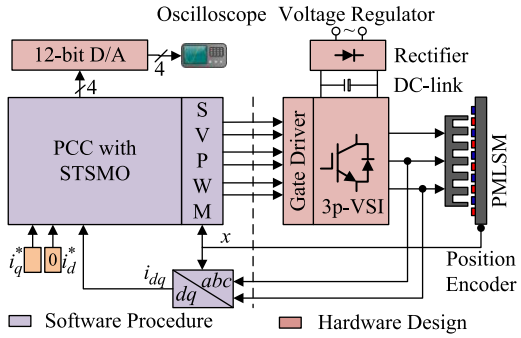

FIGURE 7. Block diagram of the experimental platform.

TABLE 1. Main parameters of PMLSM.

Symbol	Values	Unit
τ	12	mm
R	6.5	Ω
L_s	35	mH
λ_f	0.24	Wb

are depicted. Then in order to solve the parameter mismatch issue, the results with the proposed PCC+STSMO method are shown, and the comparative results between the second-order and third-order STSMO are also given and discussed. To fully prove the correctness of the proposed method, what is more, the experiments of PCC+STSMO with the different current commands are also been carried out.

Fig. 8 shows the q-axis current tracking performance of PCC under the parameter match. It can be seen that the PCC method has an ideal current tracking performance. The actual current can track the command with zero steady-state error. Furthermore, unlike PI control, the overshoot phenomenon does not happen.

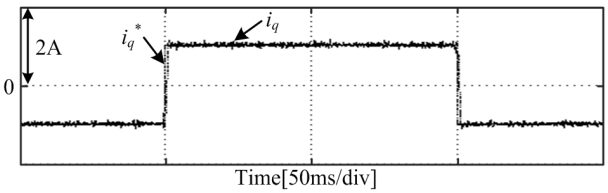

FIGURE 8. Tracking performance of PCC under the parameter match.

According to the above theoretical analysis, the parameter variations may lead to the performance degradation. Fig. 9 shows the experimental result under the resistance variation ($R_o = 2R$). There is a steady-state error in the q-axis current response after the tracking current reaches the steady-state, which is consistent with the theoretic conclusion.

Fig. 10 shows the experimental result under the inductance variation ($L_{so} = 2L_s$). It is clear that an oscillation phenomenon appears when the inductance value set in the controller is larger than the actual one. Hence a large inductance

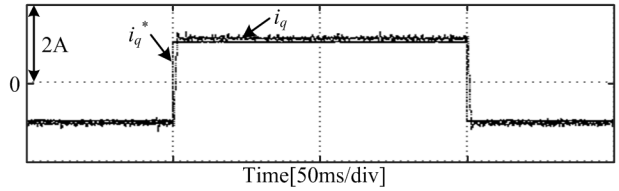

FIGURE 9. Tracking performance of PCC under $R_o = 2R$ without the compensation.

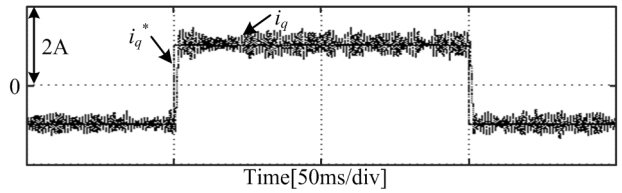

FIGURE 10. Tracking performance of PCC under $L_{so} = 2L_s$ without the compensation.

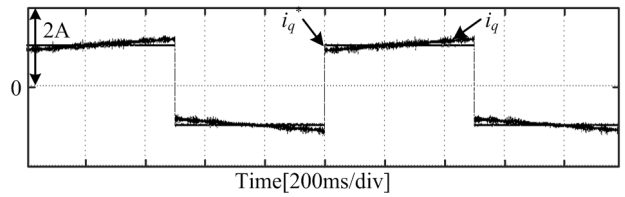

FIGURE 11. Tracking performance of PCC under $\lambda_{fo} = 2\lambda_f$ without the compensation.

set value may make the system unstable, which is a serious problem for the PCC.

Fig. 11 shows the experimental result under the flux linkage variation ($\lambda_{fo} = 2\lambda_f$). Obviously, the tracking error is related to the actual velocity, and there is a proportional relationship between the tracking error and the velocity.

To verify the correctness of the designed STSMO, Fig. 12 shows the results of the q-axis current tracking performance of PCC under different parameter variations with the second-order STSMO. The second-order STSMO parameters are set as $k_1 = 40$, and $k_2 = 14000$. Fig. 12(a) shows the compensation result under the resistance variation. Compared with Fig. 9, the steady-state error is zero, and the estimated disturbance voltage is about 6.5 [V], which is consistent with the calculation value in (14). Fig. 12(b) shows the compensation result under the inductance variation. It does not have the oscillation phenomenon, and just has an overshoot caused by the compensation process. In Fig. 12(b), we can see the disturbance voltage suddenly increases at the moment of the q-axis current change. After the compensation, the dynamic tracking performance is significantly improved, and the unstable situation disappears. Fig. 12(c) shows the compensation result under the flux linkage variation. The estimated disturbance voltage linearly increases or decreases with the acceleration or deceleration. Finally, through the

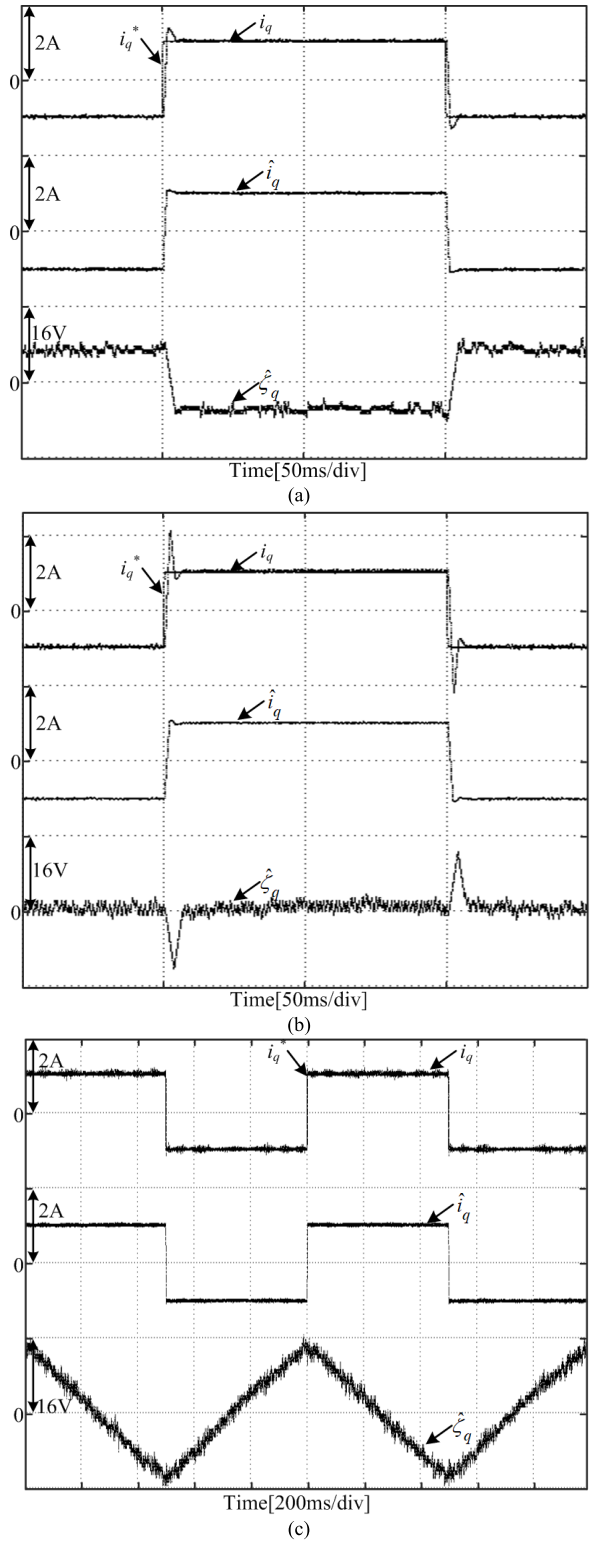

FIGURE 12. Tracking performance of PCC under the parameter variations with the second-order STSMO. (a) $R_o = 2R$. (b) $L_{so} = 2L_s$. (c) $\lambda_{fo} = 2\lambda_f$.

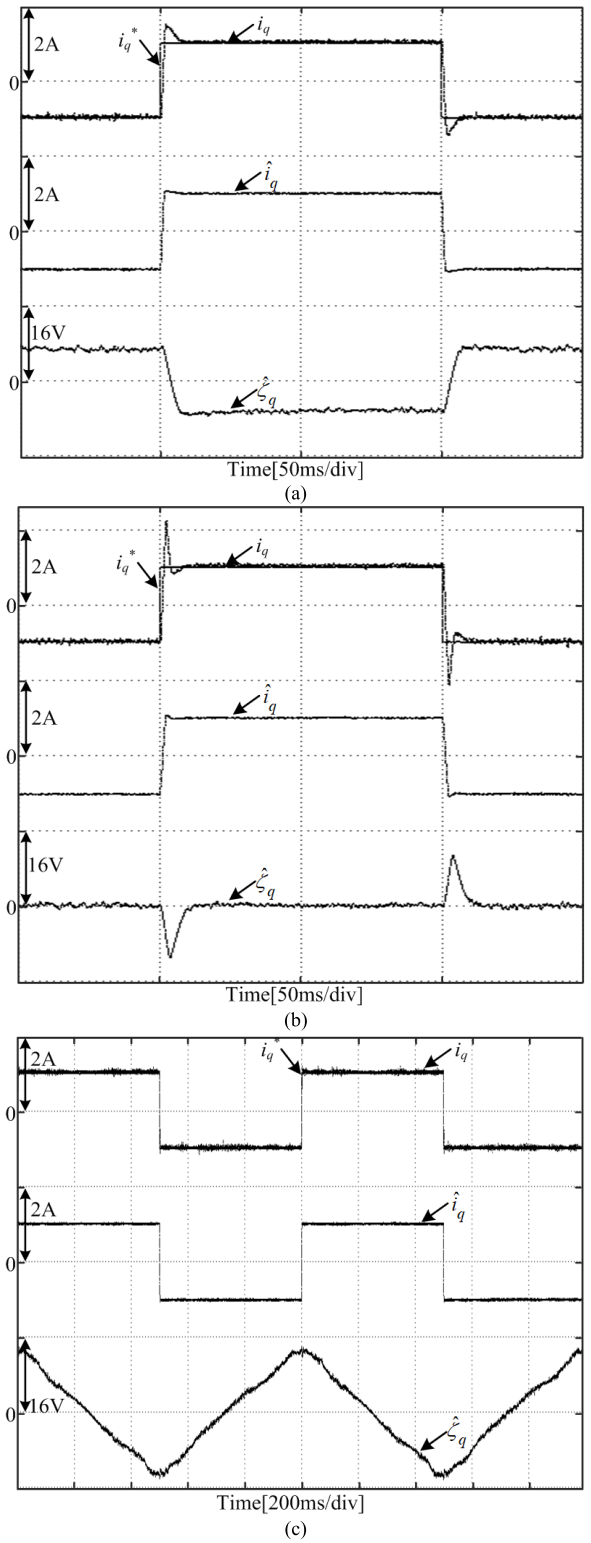

FIGURE 13. Tracking performance of PCC under the parameter variations with the third-order STSMO. (a) $R_o = 2R$. (b) $L_{so} = 2L_s$. (c) $\lambda_{fo} = 2\lambda_f$.

estimation of the second-order STSMO, the error caused by the flux linkage variation is obviously eliminated. Apart from the estimation of parameter variation, the estimation results of the q-axis current are also very accurate, and the estimation values can be used to solve the one-step delay issue.

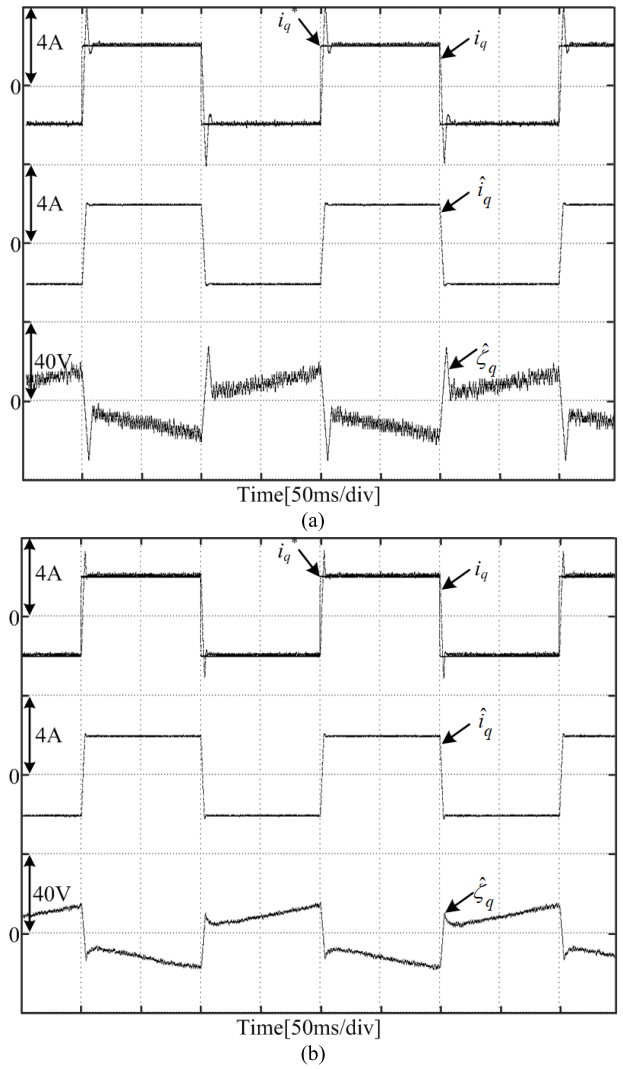

FIGURE 14. Tracking performance of PCC under the parameter variations ($R_o = 2R$, $L_{so} = 2L_s$, $\lambda_{fo} = 2\lambda_f$) with different STSMOs. (a) Second-order STSMO (b) Third-order STSMO.

Compared with Fig. 12, Fig. 13 shows the results of the tracking performance with the third-order STSMO. The third-order STSMO parameters are set as $k_1 = 40, k_2 = 14000$, and $k_3 = 50000$. It is obvious that the performance degradation caused by parameter variations is also suppressed. Beyond that, the chattering caused by the SM algorithm is dramatically reduced by the constructed third-order STSMO, which will contribute to reduce the electromagnetic noise.

To further prove the universal applicability of the proposed method, the amplitude of the current command changes from 1 [A] to 2 [A], and Fig. 14 shows the compensation results of the PCC method under parameter variations ($R_o = 2R$, $L_{so} = 2L_s$, $\lambda_{fo} = 2\lambda_f$) with two kinds of STSMO. It can be seen that the PCC with the third-order STSMO has a better tracking performance regardless of the parameter disturbance problem or chattering problem. Therefore, the proposed PCC with the third-order STSMO has the excellent performance.

To express the proposed method clearer, the comparison results between PCC without any compensation and PCC+STSMO are summarized in Table 2.

TABLE 2. Comparison results between PCC and PCC+STSMO.

Parameter situation	Performance of PCC	Performance of PCC+STSMO
$R_o = 2R$	Steady-state error	No steady-state error
$L_{so} = 2L_s$	Unstable	Stable
$\lambda_{fo} = 2\lambda_f$	Error increasing with velocity increasing	No steady-state error

Furthermore, we also compare PI control with the proposed PCC+STSMO. Firstly, the control performance for different current commands with the same PI gains is shown in Fig. 15. The command is a step signal, and the controller with the same set of parameters ($k_p = 30, k_i = 0.02$). It is clear that tracking performance becomes worse when the amplitude of the command increases, which means this set of parameters under different operating conditions is not optimal all the time.

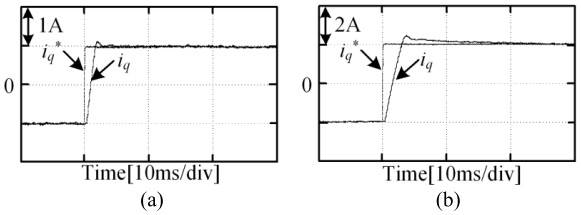

FIGURE 15. Step tracking test for different command amplitudes with the same PI parameters ($k_p = 30, k_i = 0.02$). (a) 1 [A]. (b) 2 [A].

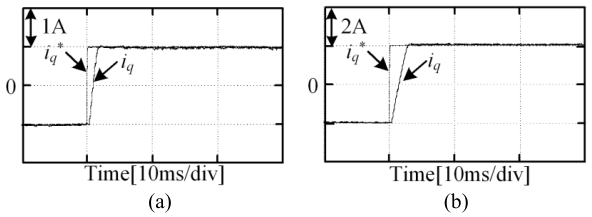

FIGURE 16. Proposed PCC for different command amplitudes. (a) 1 [A]. (b) 2 [A].

Fig. 16 shows the proposed PCC method for different command amplitudes. Different from PI Control, the tracking performance is not influenced by the variation of the command amplitude. Therefore, PCC with the parameter robustness has the better control performance than PI.

VI. CONCLUSIONS

This paper has proposed a high-performance current closed-loop with the PCC+STSMO scheme. For the one-step delay and parameter mismatch issues of the conventional PCC, they can be effectively eliminated by the proposed control scheme. Especially, the constructed STSMO is not only

to observe the d-q axis currents, which are used in the solution of one-step delay problem, but also to accurately estimate the parameter disturbance voltage. Thereby the perfect combination between PCC and STSMO can introduce a high-bandwidth and strong robust current control strategy for PMLSM drives. In addition, through designing the third-order STSMO, the chattering effect can be obviously suppressed, and a better observation can be achieved. According to the experimental results, under different parameter variations, the presented PCC+STSMO method can always acquire a good static and dynamic performance.

REFERENCES

[1] K. Sato, M. Katori, and A. Shimokohbe, "Ultrahigh-acceleration moving-permanent-magnet linear synchronous motor with a long working range," *IEEE/ASME Trans. Mechatronics*, vol. 18, no. 1, pp. 307–315, Feb. 2013.

[2] M. Y. Wang, R. Yang, C. M. Zhang, J. W. Cao, and L. Y. Li, "Inner-loop design for PMLSM drives with thrust ripple compensation and high-performance current control," *IEEE Trans. Ind. Electron.*, to be published, doi: 10.1109/TIE.2018.2814014.

[3] S. S. Ahmad and G. Narayanan, "Linearized modeling of switched reluctance motor for closed-loop current control," *IEEE Trans. Ind. Appl.*, vol. 52, no. 4, pp. 3146–3158, Jul./Aug. 2016.

[4] W. Jiang, P. Wang, Y. Ni, J. Wang, L. Wang, and Y. Liao, "Multimode current hysteresis control for brushless DC motor in motor and generator state with commutation torque ripple reduction," *IEEE Trans. Ind. Electron.*, vol. 64, no. 4, pp. 2975–2985, Apr. 2018.

[5] F. Wu, F. Feng, L. Luo, J. Duan, and L. Sun, "Sampling period online adjusting-based hysteresis current control without band with constant switching frequency," *IEEE Trans. Ind. Electron.*, vol. 62, no. 1, pp. 270–277, Jan. 2015.

[6] M. P. Kazmierkowski and L. Malesani, "Current control techniques for three-phase voltage-source PWM converters: A survey," *IEEE Trans. Ind. Electron.*, vol. 45, no. 5, pp. 691–703, Oct. 1998.

[7] M. Comanescu, L. Xu, and T. D. Batzel, "Decoupled current control of sensorless induction-motor drives by integral sliding mode," *IEEE Trans. Ind. Electron.*, vol. 55, no. 11, pp. 3836–3845, Nov. 2008.

[8] R. Yang, M.-Y. Wang, L.-Y. Li, C.-M. Zhang, and J.-L. Jiang, "Robust predictive current control with variable-gain adaptive disturbance observer for PMLSM," *IEEE Access*, vol. 6, pp. 13158–13169, Mar. 2018.

[9] M. Yang, X. Lang, J. Long, and D. Xu, "Flux immunity robust predictive current control with incremental model and extended state observer for PMSM drive," *IEEE Trans. Power Electron.*, vol. 32, no. 12, pp. 9267–9279, Dec. 2017.

[10] Y. A.-R. I. Mohamed and E. F. El-Saadany, "Robust high bandwidth discrete-time predictive current control with predictive internal model—A unified approach for voltage-source PWM converters," *IEEE Trans. Power Electron.*, vol. 23, no. 1, pp. 126–136, Jan. 2008.

[11] M. W. Naouar, A. A. Naassani, E. Monmasson, and I. Slama-Belkhodja, "FPGA-based predictive current controller for synchronous machine speed drive," *IEEE Trans. Power Electron.*, vol. 23, no. 4, pp. 2115–2126, Jul. 2008.

[12] J. Yang, W.-H. Chen, S. Li, L. Guo, and Y. Yan, "Disturbance/uncertainty estimation and attenuation techniques in PMSM drives—A survey," *IEEE Trans. Ind. Electron.*, vol. 64, no. 4, pp. 3273–3285, Apr. 2017.

[13] M. Preindl, "Robust control invariant sets and Lyapunov-based MPC for IPM synchronous motor drives," *IEEE Trans. Ind. Electron.*, vol. 63, no. 6, pp. 3925–3933, Jun. 2016.

[14] M. H. Khooban, N. Vafamand, T. Niknam, T. Dragicevic, and F. Blaabjerg, "Model-predictive control based on Takagi-Sugeno fuzzy model for electrical vehicles delayed model," *IET Electr. Power Appl.*, vol. 11, no. 5, pp. 918–934, May 2017.

[15] M. H. Khooban, N. Vafamand, and T. Niknam, "T-S fuzzy model predictive speed control of electrical vehicles," *ISA Trans.*, vol. 64, pp. 231–240, Sep. 2016.

[16] P. Wipasuramonton, Z. Q. Zhu, and D. Howe, "Predictive current control with current-error correction for PM brushless AC drives," *IEEE Trans. Ind. Appl.*, vol. 42, no. 4, pp. 1071–1079, Jul. 2006.

[17] M. Siami, D. A. Khaburi, A. Abbaszadeh, and J. Rodríguez, "Robustness improvement of predictive current control using prediction error correction for permanent-magnet synchronous machines," *IEEE Trans. Ind. Electron.*, vol. 63, no. 6, pp. 3458–3466, Jun. 2016.

[18] A. Rahimi, F. Bavafa, S. Aghababaei, M. H. Khooban, and S. V. Naghavi, "The online parameter identification of chaotic behaviour in permanent magnet synchronous motor by self-adaptive learning bat-inspired algorithm," *Int. J. Elect. Power Energy Syst.*, vol. 78, pp. 285–291, Jun. 2016.

[19] K.-H. Kim, H.-S. Kim, and M.-J. Youn, "An improved stationary-frame-based current control scheme for a permanent-magnet synchronous motor," *IEEE Trans. Ind. Electron.*, vol. 50, no. 5, pp. 1065–1068, Oct. 2003.

[20] J. Ren, Y. Ye, G. Xu, Q. Zhao, and M. Zhu, "Uncertainty-and-disturbance-estimator-based current control scheme for PMSM drives with a simple parameter tuning algorithm," *IEEE Trans. Power Electron.*, vol. 32, no. 7, pp. 5712–5722, Jul. 2017.

[21] T. Türker, U. Buyukkeles, and A. F. Bakan, "A robust predictive current controller for PMSM drives," *IEEE Trans. Ind. Electron.*, vol. 63, no. 6, pp. 3906–3914, Jun. 2016.

[22] X. Zhang, B. Hou, and Y. Mei, "Deadbeat predictive current control of permanent-magnet synchronous motors with stator current and disturbance observer," *IEEE Trans. Power Electron.*, vol. 32, no. 5, pp. 3818–3834, May 2017.

[23] J. Yang, S. Li, and X. Yu, "Sliding-mode control for systems with mismatched uncertainties via a disturbance observer," *IEEE Trans. Ind. Electron.*, vol. 60, no. 1, pp. 160–169, Jan. 2013.

[24] R. Cui, L. Chen, C. Yang, and M. Chen, "Extended state observer-based integral sliding mode control for an underwater robot with unknown disturbances and uncertain nonlinearities," *IEEE Trans. Ind. Electron.*, vol. 64, no. 8, pp. 6785–6795, Aug. 2017.

[25] D. Ginoya, P. D. Shendge, and S. B. Phadke, "Sliding mode control for mismatched uncertain systems using an extended disturbance observer," *IEEE Trans. Ind. Electron.*, vol. 61, no. 4, pp. 1983–1992, Apr. 2014.

[26] B. Wang, Z. Dong, Y. Yu, G. Wang, and D. Xu, "Static-errorless deadbeat predictive current control using second-order sliding-mode disturbance observer for induction machine drives," *IEEE Trans. Power Electron.*, vol. 33, no. 3, pp. 2395–2403, Mar. 2018.

[27] Y. Jiang, W. Xu, C. Mu, and Y. Liu, "Improved deadbeat predictive current control combined sliding mode strategy for PMSM drive system," *IEEE Trans. Veh. Technol.*, vol. 67, no. 1, pp. 251–263, Jan. 2018.

[28] A. Chalanga, S. Kamal, L. M. Fridman, B. Bandyopadhyay, and J. A. Moreno, "Implementation of super-twisting control: Super-twisting and higher order sliding-mode observer-based approaches," *IEEE Trans. Ind. Electron.*, vol. 63, no. 6, pp. 3677–3685, Jun. 2016.

[29] A. Levant, "Robust exact differentiation via sliding mode technique," *Automatica*, vol. 34, no. 3, pp. 379–384, 1998.

[30] J. Davila, L. M. Fridman, and A. Levant, "Second-order sliding-mode observer for mechanical systems," *IEEE Trans. Autom. Control*, vol. 50, no. 11, pp. 1785–1789, Nov. 2005.

[31] J. A. Moreno and M. Osorio, "Strict Lyapunov functions for the super-twisting algorithm," *IEEE Trans. Autom. Control*, vol. 57, no. 4, pp. 1035–1040, Apr. 2012.

[32] F. A. Ortiz-Ricardez, T. Sánchez, and J. A. Moreno, "Smooth Lyapunov function and gain design for a second order differentiator," in *Proc. 54th IEEE Conf. Decis. Control*, Osaka, Japan, Dec. 2015, pp. 5402–5407.

[33] A. Levant, "Higher-order sliding modes, differentiation and output-feedback control," *Int. J. Control*, vol. 76, nos. 9–10, pp. 924–941, Jan. 2003.

[34] J. A. Moreno, "Lyapunov function for Levant's second order differentiator," in *Proc. 54th IEEE Conf. Decis. Control*, Maui, HI, USA, Dec. 2012, pp. 6448–6453.

MING-YI WANG was born in Jilin, China. He received the B.E., M.E., and Ph.D. degrees in electrical engineering from the Harbin Institute of Technology (HIT), Harbin, China, in 2009, 2011, and 2016, respectively.

He is currently with the Institute of Electromagnetic and Electronic Technology, HIT. His research interests include motor drive control, power electronic applications, and magnetic levitation.

RUI YANG (S'16) was born in Suizhou, Hubei, China. He received the B.E. degree in electrical engineering from the Harbin Institute of Technology (HIT), Harbin, China, 2015, where he is currently pursuing the Ph.D. degree in electrical engineering.

His research interests include linear motor drive and control, predictive current control, adaptive control, and sliding mode control.

QIANG TAN received the B.E. and M.E. degrees in electrical engineering from the Nanjing University of Aeronautics and Astronautics, Nanjing, China, in 2014 and 2017, respectively. He is currently pursuing the Ph.D. degree with the School of the Harbin Institute of Technology.

His current research interest is design of linear permanent magnet synchronous motors.

JI-WEI CAO received the B.E. and M.E. degrees in electrical engineering from the Shenyang University of Technology, Shenyang, China, in 2005 and 2008, respectively, and the D.E. degree in electrical engineering from the Harbin Institute of Technology (HIT), Harbin, China, in 2014. He is currently with the Institute of Electromagnetic and Electronic Technology, HIT.

His research areas include high speed motor design and superconducting motor design.

CHENG-MING ZHANG was born in Harbin, China. He received the B.E., M.E., and D.E. degrees from the Harbin Institute of Technology (HIT), China, in 2005, 2007, and 2013, respectively. Since 2013, he has been a Lecturer with the School of Electrical Engineering and Automation, HIT.

His research areas include high efficiency motor systems and energy conversion and control.

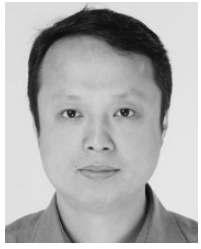

LI-YI LI (M'09) received the B.E., M.E., and D.E. degrees from the Harbin Institute of Technology (HIT), Harbin, China, in 1991, 1995, and 2001, respectively. Since 2004, he has been a Professor with the School of Electrical Engineering and Automation, HIT.

In 2013, he became Yangtze Fund Scholar Distinguished Professor and is currently supported by the National Science Fund for Distinguished Young Scholars. He has authored or co-authored over 110 technical papers and is the holder of 50 patents. His research interests include design, drive and control of linear motors, design and drive of high-speed/power density permanent magnet machines.